Polarization Switching Between Electric and Magnetic Quasi-Trapped Modes in Bianisotropic All-Dielectric Metasurfaces

Andrey B. Evlyukhin,* Maria A. Poleva, Alexei V. Prokhorov, Kseniia V. Baryshnikova, Andrey E. Miroshnichenko, and Boris N. Chichkov

A general strategy for the realization of electric and magnetic quasi-trapped modes located at the same spectral position is presented. This strategy's application makes it possible to design metasurfaces allowing switching between the electric and magnetic quasi-trapped modes by changing the polarization of the incident light wave. The developed strategy is based on two stages: the application of the dipole approximation for determining the conditions required for the implementation of trapped modes at certain spectral positions and the creation of the energy channels for their excitation by introducing a weak bianisotropy in nanoparticles. Since excitation of trapped modes results in a concentration of electric and magnetic energies in the metasurface plane, the polarization switching provides possibilities to change and control the localization and distribution of optical energy at the sub-wavelength scale. A practical method for spectral tuning of quasi-trapped modes in metasurfaces composed of nanoparticles with a preselected shape is demonstrated. As an example, the optical properties of a metasurface composed of silicon triangular prisms are analyzed and discussed.

1. Introduction

Manipulations and control of strong light-matter interactions in artificial nanoparticle structures are in the focus of current research activities. One approach is based on the resonant single-particle responses, including localized surface plasmon and Mie resonances of metal[1–3] and dielectric[4–6] nanoparticles, correspondingly. Another approach is based on the collective resonances of nanoparticle structures, and their periodic arrays.[7–9] Since resonant responses are associated with the excitation of strong electromagnetic fields in and around the nanoparticles and nanoparticle structures, modern nanophotonics is mainly focused on investigations of resonant light-matter interactions. The development and applications of resonant responses significantly depend on the absorption properties of nanostructures. In contrast to plasmonic structures, where light absorption is one of the main mechanisms of energy losses, resonant dielectric nanostructures allow accumulation and concentration of optical energy at the nanoscale with negligible losses. The efficiency of light energy concentration in dielectric nanostructures depends on the individual nanoresonators' quality factor (Q-factor) and the nanostructure's collective resonances. Recently it has been shown that all-dielectric structures and 2D nanoparticles arrays (metasurfaces) can support ultra-narrow resonances associated with, so-called, trapped modes or bound states in the continuum (BICs).[10–15] The trapped modes or BICs are protected

A. B. Evlyukhin, B. N. Chichkov
Institute of Quantum Optics
Leibniz Universität Hannover
Welfengarten Street 1, Hannover 30167, Germany
E-mail: a.b.evlyukhin@daad-alumni.de

M. A. Poleva, K. V. Baryshnikova
Faculty of Physics and Engineering
ITMO University
Saint Petersburg 197101, Russia

The ORCID identification number(s) for the author(s) of this article can be found under https://doi.org/10.1002/lpor.202100206

A. V. Prokhorov
Center for Photonics and 2D Materials
Moscow Institute of Physics and Technology
9 Institutsky Lane, Dolgoprudny 141700, Russia

A. V. Prokhorov
Department of Physics and Applied Mathematics
Vladimir State University named after Alexander and Nikolay Stoletovs
Vladimir 600000, Russia

A. E. Miroshnichenko
School of Engineering and Information Technology
University of New South Wales Canberra
Australian Capital Territory 2600, Australia

B. N. Chichkov
P.N. Lebedev Physical Institute of the Russian Academy of Sciences
Moscow 119333, Russia

eigenmodes of optical systems remaining perfectly localized without radiation into free space.[16] This provides infinite Q-factor resonances and perfect confinement of optical energy and makes these modes very attractive from fundamental and application perspectives.[17–19] True optical trapped modes are theoretical objects that can only be realized in ideal lossless infinite structures. In real practical cases, similar states can be obtained by distortion or perturbation of ideal structures' configuration properties. In this case, the trapped modes are converted into quasi-trapped modes (quasi-BICs).[20] The excitation of quasi-trapped modes leads to a high Q-factor resonance in the transmission and reflection spectra[21] and strong near-field enhancement, which may initiate the lasing,[22] nonlinear,[23] and thermal[24] processes in the nanostructure.

In this paper, a general strategy for realizing electric and magnetic quasi-trapped modes located at the same spectral position is developed. We focus on the design and theoretical investigations of metasurfaces allowing the switching between the electric and magnetic quasi-trapped modes by changing the incident light wave's polarization. This opens up new possibilities for the concentration and control of electromagnetic energy at the subwavelength scale. We consider quasi-trapped modes, which can also exist in finite-size nanostructures and metasurfaces, which is essential for experimental verification of the obtained theoretical results.

2. Electric and Magnetic Trapped Modes

In order to realize polarization switching, the physical mechanisms leading to the existence of electric and magnetic trapped modes should be clarified. Numerical calculations are not suitable for this purpose because of their implicit formalization. Therefore, we apply an analytical approach based on the multipole technique. In this case, each particle in the metasurface is replaced by its multipole moments located at the center of mass. When the particle size is small enough compared to the incident electromagnetic wave's wavelength, the multipole representation can be limited only by the dipole terms. The optical properties of such particles are determined by their electric $\widehat{\alpha}^e$ and magnetic $\widehat{\alpha}^m$ dipole polarizability tensors.

2.1. Trapped Modes as Symmetry Protected BICs

We consider an infinite metasurface with a square elementary cell composed of identical dipole particles irradiated by a monochromatic light plane wave at normal incidence. In this conditions, all particles have the same electric **p** and magnetic **m** dipole moments satisfying the following equations [25]

$$(\widehat{1} - \widehat{\alpha}^e \widehat{S}^e)\mathbf{p} = \varepsilon_0 \varepsilon_S \widehat{\alpha}^e \mathbf{E} \tag{1}$$

$$(\widehat{1} - \widehat{\alpha}^m \widehat{S}^m)\mathbf{m} = \widehat{\alpha}^m \mathbf{H} \tag{2}$$

where **E** and **H** are the external electric and magnetic fields of the incident wave in the metasurface plane, ε_0 and ε_S are the vacuum permittivity and relative dielectric permittivity of the surrounding medium, $\widehat{S}^e$ and $\widehat{S}^m$ are the tensors of electric and magnetic dipole

sums accounting for the electromagnetic interaction between the dipoles arranged into a periodic lattice of the metasurface, $\widehat{1}$ is the unit 3×3 tensor. Note that the above equations correspond to a local response theory where the dipole moments are determined by local fields and do not depend on their spatial derivatives[26] (an extended model with nonlocal bianisotropic responses will be given below). In the international system of units, one has $\widehat{S}^m = \widehat{S}^e \equiv \widehat{S}$. These dipole sums depend on the metasurface period d, the incident wavelength λ in the surrounding medium, but are independent on particle characteristics and properties, so that $\widehat{S} = \widehat{S}(d, \lambda)$. Assuming that the metasurface lattice is located in the xy plane at $z = 0$ of the Cartesian coordinate system, due to the lattice periodicity in the x and y directions, the tensor $\widehat{S}$ becomes diagonal with the non-zero elements S_{xx}, S_{yy}, and S_{zz}.[25,27] Moreover, for metasurfaces with a square elementary cell the condition $S_{xx} = S_{yy} \equiv S_\parallel$ is satisfied. We assume also that the particle polarizabilities are diagonal matrices with the elements α_{xx}^e, α_{yy}^e, and α_{zz}^e for $\widehat{\alpha}^e$ and α_{xx}^m, α_{yy}^m, and α_{zz}^m for $\widehat{\alpha}^m$. In general, these elements' values can depend on the particle shape, size, and dielectric permittivity, and the incident light wavelength.

The trapped modes (symmetry-protected BICs) of the metasurfaces correspond to solutions of Equations (1) and (2) in the absence of external fields.[28] These modes are localized within the metasurface and are not able to emit energy in the far field zone.[29] Assuming zero external fields, we obtain from Equations (1) and (2)

$$\left(\frac{1}{\alpha_\parallel^e} - S_\parallel\right) p_\parallel = 0 \,, \quad \left(\frac{1}{\alpha_\parallel^m} - S_\parallel\right) m_\parallel = 0 \tag{3}$$

$$\left(\frac{1}{\alpha_{zz}^e} - S_z\right) p_z = 0 \,, \quad \left(\frac{1}{\alpha_{zz}^m} - S_z\right) m_z = 0 \tag{4}$$

where $\alpha_\parallel$, $p_\parallel$, and $m_\parallel$ are the corresponding in-plane (in the xy-plane) components of the polarizabilities and dipole moments. As has been discussed in Subsection VIII.B of ref. [30], in a non-diffractive regime, when the metasurface period is smaller than the incident wavelength, Equation (3) have only trivial solutions ($p_\parallel = 0$ and $m_\parallel = 0$). Therefore, no trapped modes can be associated solely with the in-plane components of the dipole moments. Unlike Equation (3), solutions to Equation (4) may differ from zero in the case of nonabsorbing dipole scatterers.[30] Conditions for the existence of non-trivial solutions can be obtained from the two independent equations

$$\frac{1}{\alpha_{zz}^e} - S_z = 0 \Rightarrow \frac{1}{\alpha_{zz}^e} = S_z \tag{5}$$

$$\frac{1}{\alpha_{zz}^m} - S_z = 0 \Rightarrow \frac{1}{\alpha_{zz}^m} = S_z \tag{6}$$

Equation (5), involving only electric dipole coupling, corresponds to an electric trapped mode, and Equation (6), involving only magnetic dipole coupling, corresponds to a magnetic trapped mode. Spectral positions of the electric and magnetic trapped modes can be found using Equations (5) and (6), respectively. From these equations, one can get an important conclusion: to
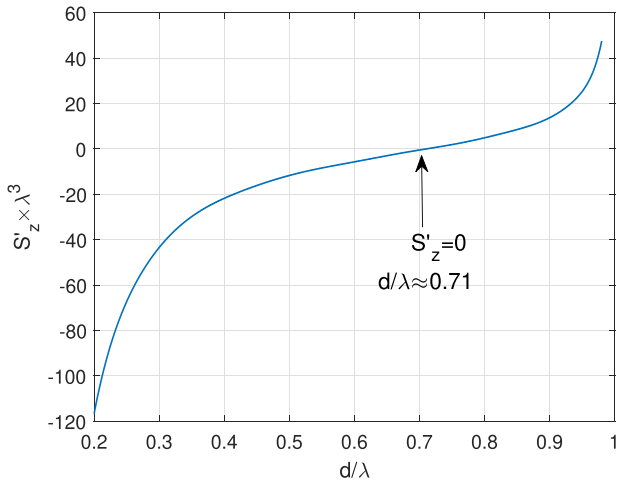
2100206 (2 of 10)

Figure 1. Real part S'_z of the dipole sum S_z calculated for different periods d of metasurfaces with square ($d \times d$) elementary cells and for a fixed wavelength ($\lambda > d$) corresponding to the wave number $k = 2\pi/\lambda$ in the medium surrounding metasurfaces.

have the trapped modes at the same spectral position, the following condition

$$\frac{1}{\alpha^e_{zz}} = \frac{1}{\alpha^m_{zz}} = S_z \tag{7}$$

should be satisfied.

Expressions for the imaginary S''_z and real S'_z parts of $S_z = S'_z + iS''_z$ are presented by

$$S'_z = \frac{k^2}{4\pi} \sum_{i=0,\pm1}^{\pm\infty} \sum_{j=0,\pm1}^{\pm\infty} \left(\frac{\cos kd_{ij}}{d_{ij}} - \frac{\sin kd_{ij}}{kd_{ij}^2} - \frac{\cos kd_{ij}}{k^2 d_{ij}^3} \right) \tag{8}$$

and

$$S''_z = \frac{k^2}{4\pi} \sum_{i=0,\pm1}^{\pm\infty} \sum_{j=0,\pm1}^{\pm\infty} \left(\frac{\sin kd_{ij}}{d_{ij}} + \frac{\cos kd_{ij}}{kd_{ij}^2} - \frac{\sin kd_{ij}}{k^2 d_{ij}^3} \right) \tag{9}$$

where $d_{ij} = d\sqrt{i^2 + j^2}$, k is the wave number in the surrounding medium, and the term with $d_{00} = 0$ is excluded from the sums. Note that Equations (8) and (9) contain explicit sum limits compared to similar equations in ref. [31]. **Figure 1** demonstrates the period behavior of normalized S'_z calculated using a method described in ref. [30]. Note that the presentation in Figure 1 does not change when the refractive index of the surrounding homogeneous medium changes. By direct analytical calculations, it is possible to show that in non-diffractive case (when $\lambda > d$ or $kd < 2\pi$) the imaginary part has the following form

$$S''_z = -k^3/(6\pi) \tag{10}$$

On the other hand, for a dielectric non-absorbing particle having diagonal tensors of the electric $\hat{\alpha}^e$ and magnetic $\hat{\alpha}^m$ dipole polarizabilties, we have from the optical theorem[30,32]

$$\Im \frac{1}{\alpha^e_{zz}} = \Im \frac{1}{\alpha^m_{zz}} = -k^3/(6\pi) \tag{11}$$

Thus, in a non-diffractive case, the condition (7) for the imaginary parts are satisfied in the spectral range where $kd < 2\pi$. In order to fulfil the condition (7) for the real parts, we can apply different tuning procedures. We can suggest three possibilities.

i) Predetermined particle. One can find the spectral point (λ'), where $\Re(\lambda'^3/\alpha^e_{zz}) = \Re(\lambda'^3/\alpha^m_{zz}) \equiv A$ for a given single particle, and then, using the curve in Figure 1, one finds the value $S'_z \times \lambda'^3 = A$ and determines the corresponding period d/λ' of the metasurfaces composed of such particles and supporting the electric and magnetic trapped modes at the same wavelength.

ii) Predetermined wavelength. For a given wavelength λ', one chooses the geometry and size of dielectric particles for which $\Re(\lambda'^3/\alpha^e_{zz}) = \Re(\lambda'^3/\alpha^m_{zz}) \equiv A$ is fulfilled, and then, using the curve in Figure 1, one finds the value $S'_z \times \lambda'^3 = A$ and determines the corresponding period d/λ' of the metasurfaces.

iii) Particle tuning (an especially resonant case). It has been shown[33,34] that by tuning the geometrical parameters of single particles, it is possible to get excitation of their electric and magnetic dipole resonances at a certain spectral position with λ_0, where $\Re(1/\alpha^e_{zz}) = \Re(1/\alpha^m_{zz}) = 0$. Therefore, for the realization of both trapped modes at this resonant condition, we can only consider the spectral position in Figure 1 corresponding to $S'_z = 0$. As a result, we get the period $d \approx 0.71\lambda_0$ for the metasurface composed of such particles and supporting the electric and magnetic trapped modes at λ_0. It is important to note that the "particle tuning" case can also be used to determine the periods of metasurfaces supporting a trapped mode of the only electric or magnetic type. To accomplish this, one should consider the electric or magnetic dipole resonant wavelength λ_0^R separately so that the corresponding period d will be equal to $0.71\lambda_0^R$ (see Figure 1).

It may happen that the period value d, determined by the suggested strategies, is smaller than the lateral (in-plane) dimensions of particles, and hence such metasurface cannot exist. In this case, the particles with other material parameters (with a higher value of the refractive index) should be considered. If the nonlocal contributions to the dipole moments are not negligible, Equations (1) and (2) will change (see the next subsection) due to the additional terms with the space derivatives of electromagnetic fields, and consequently, conditions for the realization of trapped modes may be modified. However, if the dipole approximation is applicable, the nonlocal corrections of the dipole zz-polarizabilities are still small in the optical range.[26]

The choice of the suggested strategy depends on the applications. For example, for (iii) strategy it is known in advance that the period of metasurfaces, supporting the trapped modes, is $\approx 0.7\lambda_0$ (where λ_0 is the wavelength corresponding to the dipole resonances of single particles and the trapped modes). It means that if we have (after an optimization procedure) nondispersive dielectric particles for which $\Re(1/\alpha^{ee}_{zz}) = \Re(1/\alpha^{mm}_{zz}) = 0$ at a certain resonant λ_0 we can redetermine (change) the value of the resonant λ_0 to another spectral range by simple proportional changes of the particle size, and then construct a metasurface with corresponding proprieties. The advantage of (i) strategy is that one does not need any additional optimization procedure for particle
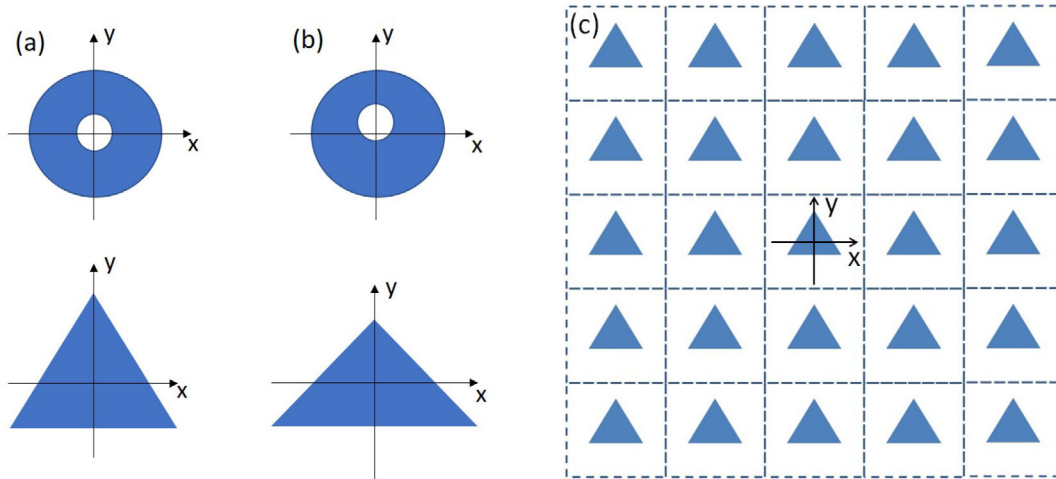
Figure 2. Top view of disks with a hole and triangular prisms: a) with and b) without rotational symmetry around the z-axis. c) Top view of a fragment of the metasurface composed of silicon prisms.

sizes and shapes. It can be used when one has a fixed set of dielectric antennas. One has to choose the antenna for which the real parts of inverse electric and magnetic dipole polarizabilities coincide at certain wavelength and then to construct the metasurface supporting the trapped modes at this wavelength. The strategy (ii) is similar to the strategy (i) but in this case we have to choose a dielectric antenna for which $\Re(1/\alpha_{zz}^{ee}) = \Re(1/\alpha_{zz}^{mm})$ is fulfilled at the required wavelength. For both (i) and (ii) cases no resonant conditions for α_{zz}^{ee} and α_{zz}^{mm} are required. Later in this article, we use strategy (i) as an example.

2.2. Quasi-Trapped Modes

The considered trapped modes correspond to the symmetry protected BICs[18,28] that cannot radiate in the far-field zone and, therefore, cannot be excited by external incident plane waves. To excite them from the far field, one has to perturb the symmetry properties of the system. One of the frequently used ways is introducing a regular asymmetric parameter characterizing the deviation of the particle shape from its symmetrical counterpart.[12,35] As a result of such transformation of particles, their dipole polarizability tensors get bianisotropic off-diagonal elements[31] as a consequence of the nonlocality of their optical response. In this case, Equations (1) and (2) are replaced by

$$(\hat{\mathbf{1}} - \hat{\alpha}^e\hat{S})\mathbf{p} - c_S^{-1}\hat{\alpha}^{em}\hat{S}\mathbf{m} = \varepsilon_0\varepsilon_S\hat{\alpha}^e\mathbf{E} + c_S^{-1}\hat{\alpha}^{em}\mathbf{H} \qquad (12)$$

$$-c_S\hat{\alpha}^{me}\hat{S}\mathbf{p} + (\hat{\mathbf{1}} - \hat{\alpha}^m\hat{S})\mathbf{m} = c_S\hat{\alpha}^{me}\mathbf{E} + \hat{\alpha}^m\mathbf{H} \qquad (13)$$

where c_S is the light velocity (in the surrounding medium with ε_S), $\hat{\alpha}^{em}$ and $\hat{\alpha}^{me}$ are the tensors of bianisotropic polarizabilities which allow excitation of the particle electric dipole by the magnetic field and the particle magnetic dipole by the electric field, correspondingly. Remind that Equations (12) and (13) are written for normal incidence of the external plane waves.

The trapped modes considered above (or the symmetry-protected BICs) arise due to the electromagnetic coupling be-

tween the corresponding out-of-plane dipole moments, that is, oriented perpendicular to the metasurface plane. However, such dipole moments cannot be excited by normally incident plane waves if the metasurface consists of particles with in-plane rotational symmetry, such as spheres, disks, cubes, cones, symmetric prisms, etc. This corresponds to the practical rule: a light plane wave does not excite the longitudinal (colinear to wave propagation) component of dipole moments of a scattering particle if the direction of its propagation coincides with the rotational symmetry axis of the particle. Therefore, in order to excite the metasurface's trapped modes, the particles' in-plane rotational symmetry must be broken. Two examples of symmetry breaking for disk and prismatic particles are shown in **Figure 2**. Introduction of such symmetry breaking leads to the appearance of bianisotropic off-diagonal polarizabilities α_{zx}^{me} and α_{zx}^{em}.[31] Applying the magnetoelectric optical theorem for particles with bianisotropic properties,[36] Equation (11) is replaced with

$$\Im\frac{1}{\alpha_{zz}^m} = -\frac{k^3}{6\pi}\left(1 + \frac{|\alpha_{zx}^{me}|^2}{|\alpha_{zz}^m|^2}\right) \qquad (14)$$

$$\Im\frac{1}{\alpha_{zz}^e} = -\frac{k^3}{6\pi}\left(1 + \frac{|\alpha_{zx}^{em}|^2}{|\alpha_{zz}^e|^2}\right) \qquad (15)$$

This indicates a distortion of the existence conditions for trapped modes compared to a metasurface with symmetric particles. As a result, the pure trapped modes are transformed into quasi-trapped modes with a finite spectral width. Nonetheless, we may expect that, because of a weak asymmetric perturbation, the second terms in the brackets of Equations (14) and (15) remain small, and the spectral positions of the magnetic and electric quasi-trapped modes can be estimated from the resonant conditions

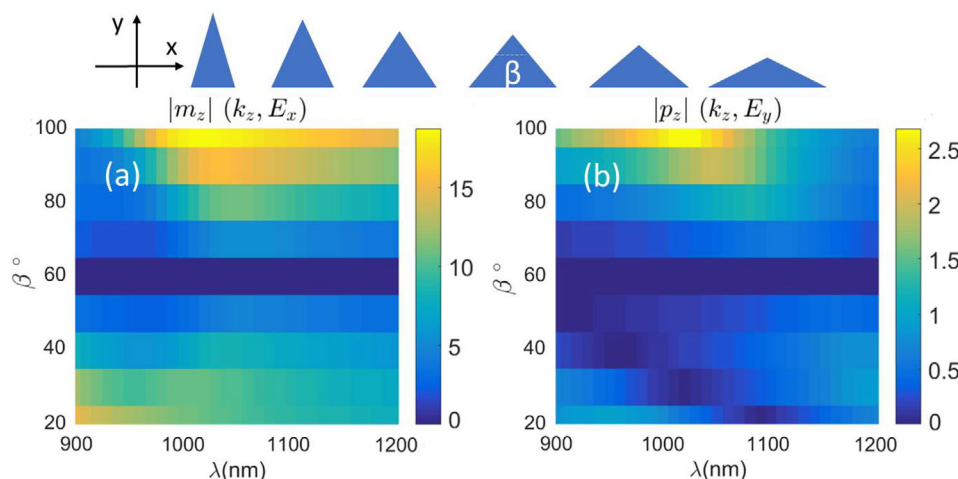$$\Re\frac{1}{\alpha_{zz}^m} = S' \quad \text{and} \quad \Re\frac{1}{\alpha_{zz}^e} = S' \qquad (16)$$

Figure 3. Absolute values (in arbitrary units) of the longitudinal (co-linear to wave propagation) z-component of the a) magnetic m_z and b) electric p_z dipole moments for silicon prisms irradiated by plane waves propagating along the z-axis and having electric polarization along a) x-axis and b) y-axis. For clarity, the inset above the main pictures illustrates the Cartesian coordinate system's orientation and changes of the prism bases with the increasing angle β. The dipole moments are calculated with respect to the prism center of mass.

respectively. Note that the quasi-trapped modes' excitation is also accompanied by strong electric and magnetic near fields in the metasurface plane.

In the following sections, we show how the discussed approach can be applied to develop metasurfaces composed of silicon triangle prisms (see Figure 2c) with a possibility of polarization switching between the electric and magnetic quasi-trapped modes in the near-infrared spectral range. To do this, we will apply the first (i) possibility described above.

3. Optical Response of Silicon Nanoprisms

We consider silicon nanoparticles in the form of triangular prisms with the relative dielectric permittivity $\varepsilon_p = 12.67$. The dimensional parameters are chosen to obtain the prism's electric and magnetic dipole responses in the near-infrared spectral range, where light absorption in silicon is negligible.[37] In this paper, the total electric field **E** in the prisms and the corresponding scattering cross sections (SCSs) are calculated numerically using the finite element method (FEM) in COMSOL Multiphysics. Then the induced polarization $\mathbf{P} = \varepsilon_0(\varepsilon_p - \varepsilon_S)\mathbf{E}$ or the displacement current density $\mathbf{j} = -i\omega\mathbf{P}$ can be calculated using the obtained field, where ω is the angular frequency and the time dependence $\exp(-i\omega t)$ is considered. After that, the multipole moments and their contributions to the SCS are calculated following the method described in ref. [38]. The Cartesian multipole moments of the scatterers are calculated following their definitions presented in ref. [39, 40]. The dipole polarizabilities are calculated using the approach described in ref. [31]. The dielectric constant $\varepsilon_S = 1$, and the electric field amplitude of the incident linear-polarized plane wave is chose to be equal 1 V m^{-1} for all simulations.

Figure 3 presents spectra of the longitudinal z-components of the magnetic and electric dipole moments excited in the prisms with different base angles β (see the inset in Figure 3) by plane waves propagating along the z-axis normally to the prism base.

All prisms have the same height and volume (the corresponding parameters for $\beta = 40°$ are shown below). One can see that the dipole z-component can be excited in all prisms except that with the equilateral triangle base ($\beta = 60°$). Notably, the type (electric or magnetic) of the dipole z-component is determined by the incident wave's polarization. For the electric- (magnetic-) polarization directed perpendicular to the bisector of the β angle, only the longitudinal z-component of the magnetic (electric) dipole moment is excited.

In the following simulations we assume that the prism bases are isosceles triangles with $\beta = 40°$ providing conditions for excitation of the z-component of electric or magnetic dipole moments by light plane waves propagating along the z-axis. In order to have the electric and magnetic dipole resonances in the spectral range $\lambda = 900$–1200 nm, we choose silicon prisms with the following geometric parameters: the prism height $H = 300$ nm, the radius of the circumscribed circle of the base triangle $R = 222$ nm, and the angle $\beta = 40°$.

In **Figure 4**a,b one can see that the SCSs are determined by only contributions of the electric ED and magnetic MD dipole terms, the contributions of the electric EQ and magnetic MQ quadruple terms are negligible. In accordance with the results in Figure 3 the waves polarized along the x-axis (perpendicular to the bisector of the β angle) generate the ED moment p_x only along the x-axis (see Figure 4c), whereas the MD moment has two components: m_y along the incident magnetic field and m_z along the wavevector of the incident light wave (see Figure 4e). For the electric y-polarization we have the MD moment m_x only along the x-axis (Figure 4f) and the ED moment has two components p_y and p_z (see Figure 4d). The longitudinal dipole components m_z and p_z are excited due to the bianisotropic response of the prism with polarizabilties α_{zx}^{me} and α_{zx}^{em}.

Figure 5a,b show that for the side irradiation the SCSs are also determined only by the ED and MD contributions. In addition, the E_z-polarized wave generates the ED $\mathbf{p} = (0, 0, p_z)$ (see Figure 5c) and the H_z-polarized wave generates the MD $\mathbf{m} = (0, 0, m_z)$ (see Figure 5d). Applying the approach described in ref.
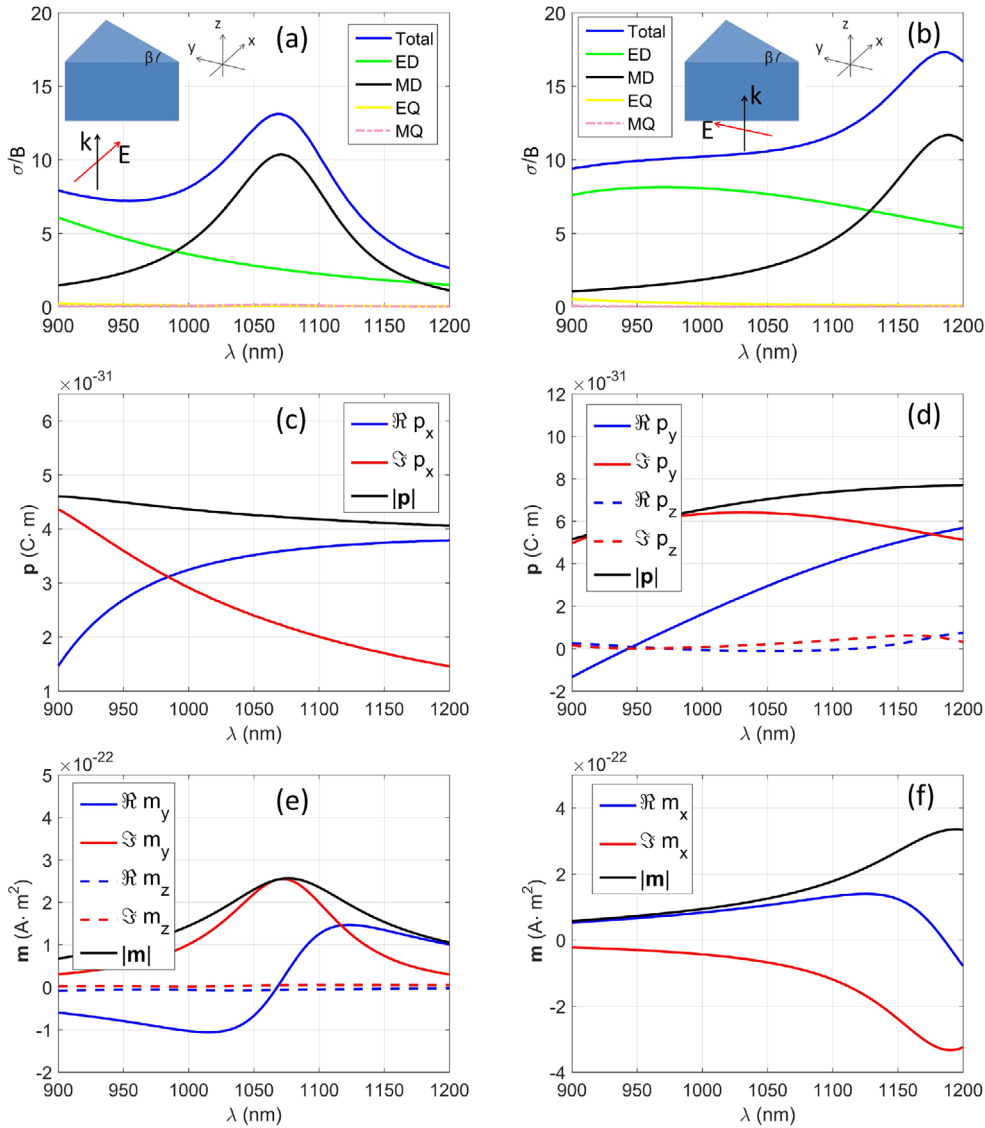
Figure 4. a,b) Spectra of the normalized scattering cross sections σ/B (where B is the area of the prism base) with corresponding multipole decomposition calculated for the silicon prism. Irradiation conditions are shown in the insets. Components of the c) electric and e) magnetic dipole moments excited in the prism at the irradiation condition shown in to the inset in (a). Components of the d) electric and f) magnetic dipole moments excited in the prism at the irradiation condition sown in the inset in (b).

[31], the polarizabilities α_{zz}^e and α_{zz}^m can be obtained from equations

$$\alpha_{zz}^e = \frac{p_z^+ + p_z^-}{2\varepsilon_0 E(0)} \tag{17}$$

and

$$\alpha_{zz}^m = \frac{m_z^+ - m_z^-}{2(\varepsilon_0/\mu_0)^{1/2} E(0)} \tag{18}$$

where μ_0 is the vacuum magnetic permeability, p_z^+ and p_z^- are the ED components obtained for the direct (along the x-axis) and inverse irradiation shown in the inset in Figure 5a (the electric polarization is the same for both incident wave directions), re-

spectively; m_z^+ and m_z^- are the MD components obtained for the direct (along the x-axis) and inverse irradiation shown in the inset in Figure 5b (again the electric polarization is the same for both incident wave directions), respectively; $E(0)$ is the incident electric field at the point of the ED and MD location (in this paper this is the electric field amplitude of the incident wave).

Spectral behavior of the normalized inverse polarizabilities is presented in **Figure 6**. The imaginary parts of λ^3/α_{zz}^e and λ^3/α_{zz}^m have the numerical value close to $(-4\pi^2/3)$ corresponding to Equations (14) and (15) with small contributions of bianisotropic (nonlocal) terms. The real parts of the normalized inverse polarizabilities intersect at the wavelength $\lambda' \approx 1025$ nm and take the value ≈ 5 (see black circle in Figure 6).

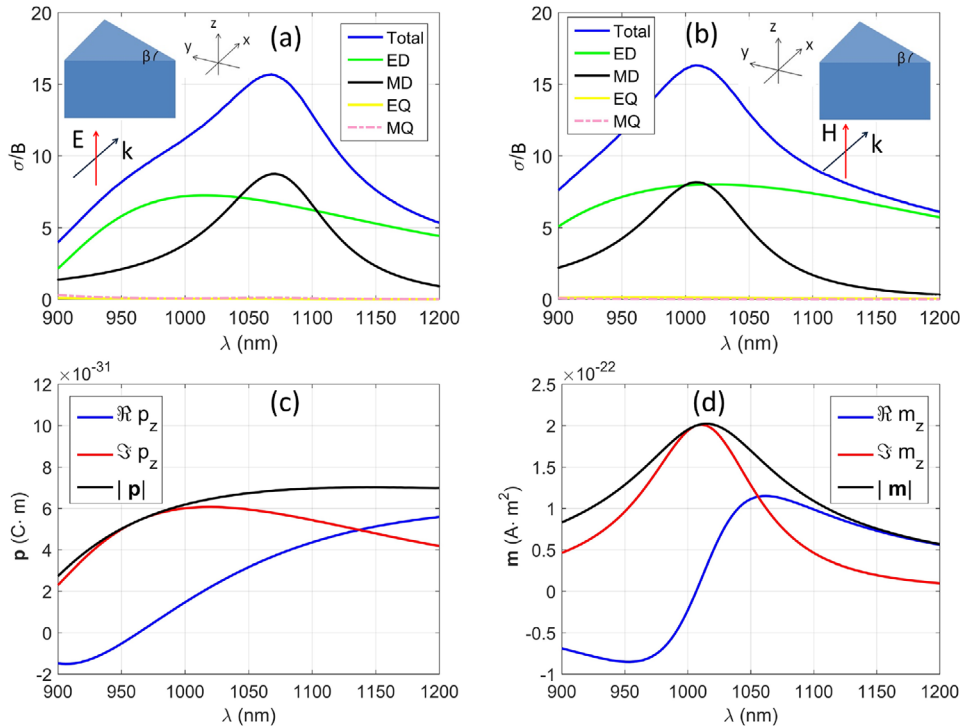To estimate the period d' of the metasurfaces composed of such prisms and supporting the electric and magnetic

ADVANCED
SCIENCE NEWS

www.advancedsciencenews.com

LASER
& PHOTONICS
REVIEWS

www.lpr-journal.org

Figure 5. a,b) Spectra of the normalized scattering cross sections σ/B (where B is the area of the prism base) with corresponding multipole decomposition calculated for the silicon prism. Irradiation conditions are shown in the insets. c) Components of the electric dipole moment excited in the prism at the irradiation condition shown in the inset in (a). d) Components of the magnetic dipole moment excited in the prism at the irradiation condition shown in the inset in (b).
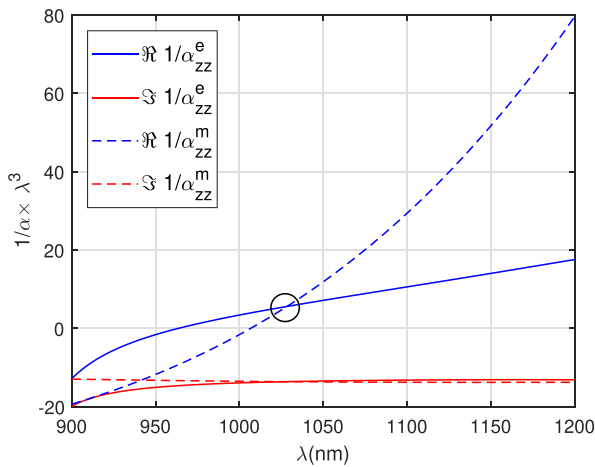

Figure 6. Normalized inverse electric and magnetic zz-polarizabilities of the prism calculated using the dipole moments presented in Figures 5c,d, respectively. The black circle indicates the point where $\Re(1/\alpha_{zz}^e) = \Re(1/\alpha_{zz}^m)$.

quasi-trapped modes at the same wavelength, we can apply the (i) procedure described above. Using Figure 1, we can find that $S_z' \times \lambda^3 = 5$ at $d/\lambda \approx 0.8$ corresponding to $d' = 0.8\lambda' = 820$ nm, where λ' corresponds to the crossing of $\Re(1/\alpha_{zz}^m)$ and $\Re(1/\alpha_{zz}^e)$ in Figure 6. The next section will show that the obtained period is

in complete agreement with the results obtained by more general full-wave numerical simulations.

4. Quasi-Trapped Modes in Metasurfaces Composed of the Prisms

The dipole method described above gives us information about the periodicity of the metasurface. However, since this is only an approximate approach, in general cases, the metasurface period may differ slightly from that obtained in the dipole approximation for bianisotropic particles. Therefore, the last stage of the proposed procedure should include numerical verification and fine-tuning of metasurface periodicity supporting polarization switching between the quasi-trapped modes.

Using the Lumerical calculation facilities, we simulate the transmission coefficients of metasurfaces composed of the prisms with parameters corresponding to Figure 5 and orientation as in Figure 2c with angle β directed along y−axis (see Figure 3). The centers of mass of every prism are located in the $z = 0$ plane. The metasurface is irradiated by normally incident light plane waves with the electric polarization directed along the x- or y-axis. The obtained results are shown in **Figure 7**. One can see that for both polarizations, the transmission spectra have narrow resonant features around $\lambda = 1000$ nm. For the period $d = 777$ nm, these resonances are spectrally separated. However, by tuning the periodicity, it is possible to keep these resonances at the same spectral positions, as shown in Figure 7b for the period $d = 820$ nm. Note that this period $d = 820$ nm coincides with the
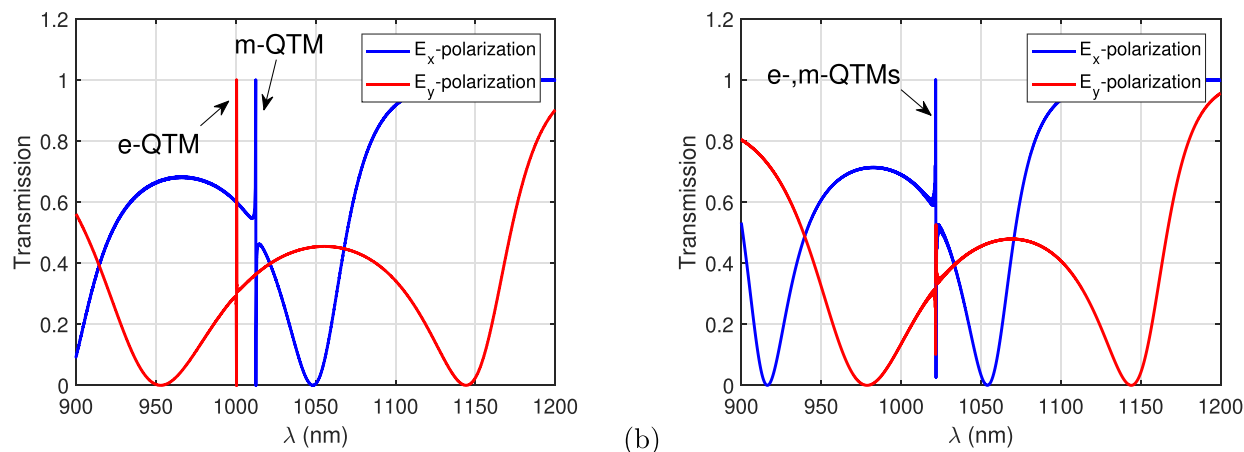
Figure 7. Numerically calculated transmission spectra of the metasurfaces composed of the silicon prisms irradiated by normally incident light plane waves with different polarizations. The metasurface periods are a) $d = 777$ nm and b) $d = 820$ nm. The arrows indicate the electric (e-QTM) and magnetic (m-QTM) quasi trapped modes (QTMs).

value $d' = 820$ nm obtained above in the dipole approximation. The estimated Q-factors of these narrow resonances reach values up to several thousands.

To prove that these resonances indeed correspond to the electric or magnetic dipole coupling, we present electric and magnetic field distributions in different planes crossing the elementary cell of the metasurface (see **Figure 8**), which are calculated at the position of narrow resonances shown in Figure 7b. In Figure 8 one can see (for the xy-plane) that for the E_y-polarization the total electric field is concentrated at the center of the prism, whereas the magnetic field is distributed like a ring around the electric field. Such distribution exactly corresponds to the ED response of the prism. For the E_x-polarization, one has an inverse situation: in the xy-plane the magnetic field is concentrated at the prism center, and the electric field has a ring distribution around the center corresponding to the MD response. Thus, at the same spectral position, polarization switching allows excitation of two resonances corresponding to the electric quasi-trapped mode (e-QTM) and magnetic quasi-trapped mode (m-QTM). One can see in Figure 8 that these modes are associated with the generation of strong electric and magnetic fields inside and around the prisms. Under the e-QTM (m-QTM) excitation, the total electric (magnetic) field has the maximum value about of 200 (300) times greater than the electric (magnetic) field of the incident wave. The spatial distribution of these fields can be controlled by the incident waves' polarization (see Figure 8).

It is important to emphasize that the metasurface period supporting the ED and MD quasi-trapped modes at a given spectral position has been determined in advance by using the polarizabilities of single prisms and the general curve shown in Figure 1.

5. Conclusion

Theoretical approach for the design of metasurfaces, supporting the electric and magnetic quasi-trapped modes (quasi-BICs) located at the same spectral position, has been developed and demonstrated. In the framework of dipole approximation, the general conditions for the realization of such modes, connecting single particles' optical properties with the metasurface lattice periodicity, have been formulated. Possibilities for tuning these modes to the required spectral position using a combination of analytical and numerical methods have been suggested. This approach has been applied for the development of metasurfaces composed of silicon triangle prisms. It has been shown that one can perform switching between the electric and magnetic quasi-trapped modes located at the same infrared spectral position by changing the incident light polarization. Since the trapped modes are associated with the excitation of strong electric and magnetic fields in the metasurface, the polarization switching opens a way to sub-wavelength manipulation of the electromagnetic fields. Moreover, using a circularly polarized wave, both quasi-trapped modes can be excited simultaneously. The suggested effects create new opportunities for the application of metasurfaces with the trapped modes in a wide electromagnetic spectral range from the optical to radio frequencies.

Conflict of Interest

The authors declare no conflict of interest.

Data Availability Statement

Research data are not shared.

ADVANCED
SCIENCE NEWS

www.advancedsciencenews.com
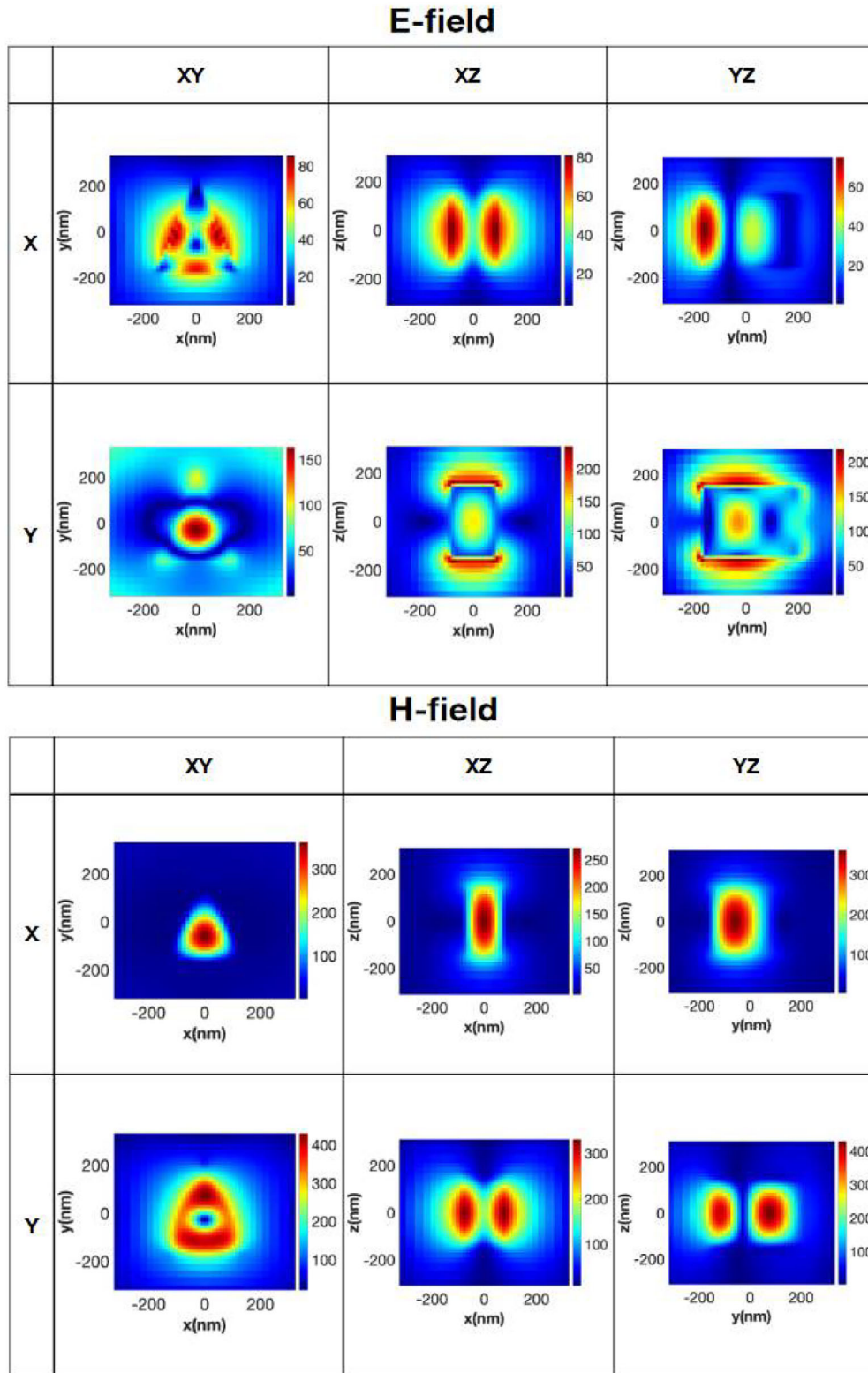
www.lpr-journal.org

LASER
& PHOTONICS
REVIEWS

Figure 8. Magnitudes of the electric and magnetic field distributions in different planes crossing the metasurface elementary cell containing the prism, which are calculated at the position of narrow resonances shown in Figure 7b. The top horizontal lines of the tables define the crossing planes. The vertical left-hand sideline defines the incident wave electric polarization. The magnitudes of the total electric and magnetic fields are normalized by the amplitudes of the incident wave's electric and magnetic fields, respectively.

[1] J. A. Schuller, E. S. Barnard, W. Cai, Y. C. Jun, J. S. White, M. L. Brongersma, *Nat. Mater.* **2010**, *9*, 193.

[2] V. Giannini, A. I. Fernández-Domínguez, S. C. Heck, S. A. Maier, *Chem. Rev.* **2011**, *111*, 3888.

[3] N. J. Halas, S. Lal, W.-S. Chang, S. Link, P. Nordlander, *Chem. Rev.* **2011**, *111*, 3913.

[4] A. B. Evlyukhin, S. M. Novikov, U. Zywietz, R. L. Eriksen, C. Reinhardt, S. I. Bozhevolnyi, B. N. Chichkov, *Nano Lett.* **2012**, *12*, 3749.

[5] P. Albella, R. Alcaraz de la Osa, F. Moreno, S. A. Maier, *ACS Photonics* **2014**, *1*, 524.

[6] Y. Yang, V. A. Zenin, S. I. Bozhevolnyi, *ACS Photonics* **2018**, *5*, 1960.

[7] B. Auguié, W. L. Barnes, *Phys. Rev. Lett.* **2008**, *101*, 143902.

[8] V. Giannini, G. Vecchi, J. G. Rivas, *Phys. Rev. Lett.* **2010**, *105*, 266801.

[9] J. Zhang, W. Liu, Z. Zhu, X. Yuan, S. Qin, *Opt. Express* **2014**, *22*, 30889.

[10] J. Zhang, K. F. MacDonald, N. I. Zheludev, *Opt. Express* **2013**, *21*, 26721.

[11] C. W. Hsu, B. Zhen, A. D. Stone, J. D. Joannopoulos, M. Soljačić, *Nat. Rev. Mater.* **2016**, *1*, 16048.

[12] V. R. Tuz, V. V. Khardikov, A. S. Kupriianov, K. L. Domina, S. Xu, H. Wang, H.-B. Sun, *Opt. Express* **2018**, *26*, 2905.

[13] K. Koshelev, S. Lepeshov, M. Liu, A. Bogdanov, Y. Kivshar, *Phys. Rev. Lett.* **2018**, *121*, 193903.

[14] S. Han, L. Cong, Y. K. Srivastava, B. Qiang, M. V. Rybin, A. Kumar, R. Jain, W. X. Lim, V. G. Achanta, S. S. Prabhu, Q. J. Wang, Y. S. Kivshar, R. Singh, *Adv. Mater.* **2019**, *31*, 37 1901921.

[15] K. Koshelev, A. Bogdanov, Y. Kivshar, *Sci. Bull.* **2019**, *64*, 836.

[16] F. Monticone, D. Sounas, A. Krasnok, A. Alu, *ACS Photonics* **2019**, *6*, 3108.

[17] D. R. Abujetas, N. van Hoof, S. ter Huurne, J. G. Rivas, J. A. Sánchez-Gil, *Optica* **2019**, *6*, 996.

[18] S. Li, C. Zhou, T. Liu, S. Xiao, *Phys. Rev. A* **2019**, *100*, 063803.

[19] S. Han, P. Pitchappa, W. Wang, Y. K. Srivastava, M. V. Rybin, R. Singh, *Adv. Opt. Mater.* **2021**, *9*, 2002001.

[20] S. Murai, D. R. Abujetas, G. W. Castellanos, J. A. Sánchez-Gil, F. Zhang, J. G. Rivas, *ACS Photonics* **2020**, *7*, 2204.

[21] D. R. Abujetas, Á. Barreda, F. Moreno, J. J. Sáenz, A. Litman, J.-M. Geffrin, J. A. Sánchez-Gil, *Sci. Rep.* **2019**, *9*, 16048.

[22] S. T. Ha, Y. H. Fu, N. K. Emani, Z. Pan, R. M. Bakker, R. Paniagua-Domínguez, A. I. Kuznetsov, *Nat. Nanotechnol.* **2018**, *13*, 1042.

[23] L. Xu, K. Zangeneh Kamali, L. Huang, M. Rahmani, A. Smirnov, R. Camacho-Morales, Y. Ma, G. Zhang, M. Woolley, D. Neshev, A. E. Miroshnichenko, *Adv. Sci.* **2019**, *6*, 1802119.

[24] K. Zangeneh Kamali, L. Xu, J. Ward, K. Wang, G. Li, A. E. Miroshnichenko, D. Neshev, M. Rahmani, *Small* **2019**, *15*, 1805142.

[25] A. B. Evlyukhin, C. Reinhardt, A. Seidel, B. S. Luk'yanchuk, B. N. Chichkov, *Phys. Rev. B* **2010**, *82*, 045404.

[26] D. A. Bobylev, D. A. Smirnova, M. A. Gorlach, *Phys. Rev. B* **2020**, *102*, 115110.

[27] V. E. Babicheva, A. B. Evlyukhin, *Phys. Rev. B* **2019**, *99*, 195444.

[28] D. R. Abujetas, J. Olmos-Trigo, J. J. Sáenz, J. A. Sánchez-Gil, *Phys. Rev. B* **2020**, *102*, 125411.

[29] C. W. Hsu, B. Zhen, A. D. Stone, J. D. Joannopoulos, M. Soljačić, *Nat. Rev. Mater.* **2016**, *1*, 16048.

[30] V. E. Babicheva, A. B. Evlyukhin, *J. Appl. Phys.* **2021**, *129*, 040902.

[31] A. B. Evlyukhin, V. R. Tuz, V. S. Volkov, B. N. Chichkov, *Phys. Rev. B* **2020**, *101*, 205415.

[32] A. Alu, N. Engheta, *Phys. Rev. B* **2006**, *74*, 205436.

[33] A. B. Evlyukhin, C. Reinhardt, B. N. Chichkov, *Phys. Rev. B* **2011**, *84*, 235429.

[34] I. Staude, A. E. Miroshnichenko, M. Decker, N. T. Fofang, S. Liu, E. Gonzales, J. Dominguez, T. S. Luk, D. N. Neshev, I. Brener, Y. Kivshar, *ACS Nano* **2013**, *7*, 7824.

[35] V. Fedotov, M. Rose, S. Prosvirnin, N. Papasimakis, N. Zheludev, *Phys. Rev. Lett.* **2007**, *99*, 147401.

[36] I. Sersic, C. Tuambilangana, T. Kampfrath, A. F. Koenderink, *Phys. Rev. B* **2011**, *83*, 245102.

[37] E. D. Palik, *Handbook of Optical Constants of Solids*, Vol. 3, Academic Press, San Diego, CA **1998**.

[38] P. D. Terekhov, K. V. Baryshnikova, Y. A. Artemyev, A. Karabchevsky, A. S. Shalin, A. B. Evlyukhin, *Phys. Rev. B* **2017**, *96*, 035443.

[39] R. Alaee, C. Rockstuhl, I. Fernandez-Corbaton, *Opt. Commun.* **2018**, *407*, 17.

[40] A. B. Evlyukhin, B. N. Chichkov, *Phys. Rev. B* **2019**, *100*, 125415.